HHS Public Access

Author manuscript

Biochemistry. Author manuscript; available in PMC 2021 March 26.

Published in final edited form as:

Biochemistry. 2021 February 02; 60(4): 289–302. doi:10.1021/acs.biochem.0c00714.

Type II Binders Targeting the "GLR-out" Conformation of the Pseudokinase STRADα

Ryan H.B. Smith[1,2], **Zaigham M. Khan**[2], **Peter Man-Un Ung**[1], **Alex Scopton**[2], **Lisa Silber**[2], **Seshat M. Mack**[1], **Alexander Real**[2], **Avner Schlessinger**[1,*], **Arvin C. Dar**[2,*]

[1]Department of Pharmacological Sciences, Icahn School of Medicine at Mount Sinai, New York, New York, USA.

[2]Department of Oncological Sciences, Icahn School of Medicine at Mount Sinai, New York, New York, USA.

Abstract

Pseudokinases play important roles in signal transduction and cellular processes similarly to catalytically competent kinases. However, pseudokinase pharmacological tractability and conformational space accessibility are poorly understood. Pseudokinases have only recently been suggested to adopt "inactive" conformations or interact with conformation specific kinase inhibitors (e.g., type II compounds). In this work, the heavily substituted pseudokinase STRADα, which possesses a DFG->GLR substitution in the catalytic site that permits nucleotide binding while impairing divalent cation coordination, is used as a test case to demonstrate the potential applicability of conformation-specific, type II compounds to pseudokinase pharmacology. Integrated structural modeling is employed to generate a "GLR-out" conformation ensemble. Likely interacting type II compounds are identified through virtual screening against this ensemble model. Biophysical validation of compound binding is demonstrated through protein thermal stabilization and ATP competition. Localization of a top-performing compound through surface methylation strongly suggests that STRADα can adopt the "GLR-out" conformation and interact with compounds that comply with the standard type II pharmacophore. These results suggest that, despite a loss of catalytic function, some pseudokinases including STRADα may retain the conformational switching properties of conventional protein kinases.

Graphiycal abstract

[*]**Corresponding Authors:** arvin.dar@mssm.edu, avner.schlessinger@mssm.edu.
Avner Schlessinger is the co-founder of AIchemy.

Supporting Information.
Experimental Methods and Supplemental Figures S1–S12 and Tables S1–S4
This material is available free of charge via the Internet at http://pubs.acs.org.

UNIPROT ACCESSION IDS
AMPK, Q13131; c-Src, P12931; ERK, P27361; KSR2, Q6VAB6; LKB1, Q15831; MARK, Q9P0L2; MO25α, Q9Y376; mTOR, P42345; STRADα, Q7RTN6; VEGFR2, P35968.

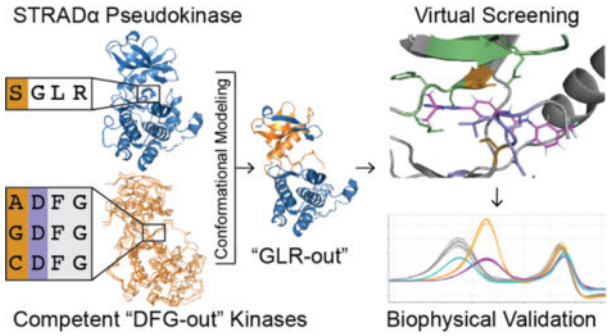

Introduction

Approximately ten percent of the human kinome is comprised of pseudokinases, a subclass of kinases that possess inactivating variations relative to the canonical kinase sequence at conserved, catalytically critical residues.[1] Despite the loss of active site residues that function in phosphoryl group transfer, pseudokinases are well-conserved and are present in all organisms that possess canonical, catalytically-competent kinases (hereafter referred to as *bona fide* kinases).[2–3] A fundamental aspect of kinases, and potentially of pseudokinases, is their role as molecular switches in both normal homeostasis and disease.[4] Pseudokinases often play an auxiliary signaling role to *bona fide* kinases: they have been shown to control key, rate-limiting steps and to serve as mechanisms for fine-tuning intracellular signaling networks.[4–5] Most characterized pseudokinases regulate signal transduction through modulation of protein-protein interactions that control the activity and cellular localization of catalytic pathway components.[4, 6] These interactions often depend on the conformation of the residues surrounding the degraded active site. This region in pseudokinases, which we refer to as the pseudocatalytic cleft,[7] corresponds to the ATP-binding site of *bona fide* kinases. The conformation of the pseudocatalytic cleft has the potential to allosterically control protein-protein interactions because the surrounding residues form parts of several of the most common canonical kinase dimerization and substrate recognition interfaces.[6, 8–9]

The kinase catalytic cleft adopts a range of active and inactive conformations that have been shown to control both the activity of the kinase itself and the formation of signaling complexes. The transitional energetics between these states are determined in large part by the proximal residues of conserved structural motifs, including the aspartate-phenylalanine-glycine (DFG) motif and the αC helix.[10] The DFG motif position has been described as essential for catalytic function through magnesium coordination and through the binding and release of nucleotide and substrate during cycles of phosphorylation.[11] In addition to its catalytic function, the DFG motif also forms the first part of the activation loop—a key regulatory element controlling both ATP-binding and accessibility of the kinase substrate recognition groove. Lacking evolutionary pressure to maintain this motif, pseudokinases frequently contain significant substitutions within this motif. Of 52 pseudokinases included in the original published human kinome, approximately half contain two or three major DFG substitutions and only seven contain none.[1]

Small molecule kinase inhibitors (KIs) have been developed that target and stabilize multiple catalytic cleft conformations. KIs are typically grouped into numbered classes based on the catalytic cleft conformation to which they bind.[10, 12–14] These inhibitor categories are associated with varying biochemical and pharmacodynamic profiles that depend on the size, hydrophobicity, and other characteristics of targeted pockets.[15] KIs that target the active state—"DFG-in/αC helix-in" conformation—are referred to as type I compounds. Current classification distinguishes at least five further categories of KIs against inactive conformations.

Two of the best studied categories are those that bind the "DFG-out" conformation (termed type II compounds) and those that bind the "αC helix-out" conformation (termed type I½ compounds). Type II KIs bind to the "DFG-out" state, stabilizing a flip of the activation loop that reveals a hydrophobic pocket and disrupts the substrate recognition groove on the front of the kinase. Incorporating hydrophobic chemical motifs in type II compounds can improve pharmacodynamic properties and target potency while drawing on more synthetic chemical space.[16] This class now includes many clinically important KIs including sorafenib, regorafenib, and imatinib. Type I½ compounds alter rotation of the αC helix and influence the adjacent dimerization domain found in many kinases. This class includes clinical drugs including dasatinib, lapatinib, and vemurafenib.

Inactive conformation-specific KIs offer an intuitive path to manipulate pseudokinase-dependent signaling because regulation of protein-protein interactions targets the core, non-catalytic functions of pseudokinases. However, pseudokinases have only been reported to interact with a small number of such inactive conformation-specific inhibitors.[12, 17] Examples include several type I½ compounds that have been shown to modulate MAPK/ERK pathway signaling through conformational control of the pseudokinase KSR2.[18–19] A type II small molecule was recently characterized with one of the pseudokinases lacking DFG motif substitutions,[17] but type II KI tolerance for DFG motif variations remains unclear. Fully 95.7% of canonical kinases in the original human kinome comply with the consensus sequence of "D[F/L/Y]G," while only 14% of pseudokinases follow this consensus.[1] No tolerance for substitutions at the conserved aspartate by any type II KI has ever been reported. Recently, KSR1/2 has been demonstrated to directly impact the pharmacology of several allosteric MEK inhibitors (MEKi), including the clinical drug trametinib, through direct contacts formed at a complex with MEK.[20] This data highlights novel modes by which pseudokinases make interact with known KIs but through previously unrecognized mechanisms.

One pseudokinase that is heavily substituted relative to the canonical kinase sequence with uncharacterized pharmacology is the STE20-related Adaptor Protein Alpha (STRADα). This protein functions by localizing and activating the serine-threonine kinase B1 (LKB1) in complex with Calcium-binding Protein 39 (MO25α).[21] STRADα binds nucleotides in a magnesium-independent manner but has multiple deficiencies in its catalytic machinery.[22] Formation of this complex translocates LKB1 from the nucleus to its downstream cytoplasmic signaling partners.[21] LKB1 activation is further dependent on critical interactions of its N-terminal lobe (N-lobe) with the activation loop of STRADα and of its αC helix with MO25α.[23] Full activation of LKB1 depends on ATP binding to STRADα.[23]

The net effect of active LKB1 signaling is to act as a tumor suppressor through the broad inhibition of cell growth, division, proliferation, migration, and anabolism.[24–25] LKB1 constrains cellular activities to available energy through the AMPK-mTOR pathway.[26–28] It further maintains cell polarity thereby preventing cells from undergoing an epithelial-mesenchymal transition through MARK-mediated signaling.[29–30] LKB1 is considered a tumor suppressor because of its constraints on proliferation and migration, but it is increasingly understood to also protect tumors from microenvironmental metabolic stress.[24]

STRADα is a particularly interesting test case for investigating pseudokinase function and pharmacology because it is among the most heavily substituted pseudokinases at the ATP-binding site. Its substitution of the DFG motif to glycine-leucine-arginine (GLR) is of note because no pseudokinase with inactivating DFG motif variations has been reported to bind type II KIs. Further, no variability in the aspartate position has been shown to be tolerated by such compounds, and only 1.1% of *bona fide* kinases even have a polar residue substituted for glycine. If STRADα were to bind type II inhibitors and exhibit altered signaling (Figure S1), it would suggest broader conservation and repurposing of this conformational cycle for alternative non-phosphorylation functions. STRADα is also appealing as a test case for compound development because it is among the least pharmacologically studied of human kinases.[31] No positive non-nucleotide interactions had been published when this project was initiated; at the time of submission, only low-confidence, unverified compounds from high throughput screens have been reported.[32]

In this work, we set out to use the pseudokinase STRADα to determine whether active site variations in pseudokinases impedes access to the “DFG-out” conformation, and whether pharmacological targeting of this conformation with type II inhibitors has potential to manipulate signaling. We evaluated the extent to which deviations from the consensus *bona fide* kinase sequence exhibited by kinases known to adopt the “DFG-out” conformation might influence the tractability of STRADα for modulation with type II compounds. We modeled STRADα in a state similar to the “DFG-out” conformation (termed the “GLR-out” conformation) and generated an ensemble model that we used to identify conformation-specific STRADα ligands. Finally, we corroborated models proposing a type II pose for a top compound through observing alterations in thermal stabilization due to surface lysine methylation.

Materials and Methods

Alignment and conservation analysis

Alignment of STRADα against active human kinases was performed using the T-Coffee 3D-Coffee alignment program on the crystallized minimal kinase domain.[33] This incorporation of structural information in the sequence alignment proved helpful in correctly aligning STRADα with *bona fide* kinases, especially tyrosine kinases, because of STRADα’s significant sequence deviations at normally conserved motifs. Representative sequences were chosen and compared at residues aligned with the human sequence at 76, 78, and 81 for conservation of the glycine rich loop, 100 for the salt bridge, 147 for the gatekeeper, 185 and 429–431 for the MO25α interaction interface, 195, 200, and 213 for magnesium and γ-

phosphate coordination, 148 and 212 for “DFG-out” conformational accessibility, 231, 233, and 251 for the LKB1 interaction interface.

This alignment was then used as the basis for the full multiple sequence alignment against all STRADα homologs identified through Pfam[34] and Treefam[35] using MAFFT and ClustalW.[36] Sequences were trimmed to the kinase domain in order to reduce noise in the alignment and make general similarity measures (e.g. for tree-building) more reflective of the particular data of interest. Analysis of this superset revealed relative evolutionary instability in simple model systems. Conservation of the WEF motif—a region previously reported to be necessary for interaction with MO25α and consequently critical for STRADα’s function as a pseudokinase—was used as a simple identifier of orthologs that might be compatible with the known biology of human STRADα. Deuterostome orthologs (equivalent in this case to chordate orthologs) structurally resembled human STRADα while protostome orthologs contained significantly greater sequence variation across the sites corresponding to protein-protein interfaces in human STRADα. This chordate subset of orthologs was used for subsequent analysis. The same cutoff was applied when selecting orthologs for the analysis of MO25α and LKB1. These alignments were used to map conservation onto the surface of the STRADα/MO25α/LKB1 complex using the ConSurf server using standard parameters.[37]

Ensemble modeling

Initial homology modeling of STRADα into the “DFG-out” conformation was performed using DFGmodel.[38] The 3GNI chain B crystal structure was aligned against 18 serine/threonine template structures using 3D-coffee (part of T-Coffee 11.0)[33] and manually edited as necessary. MODELLER 9.17[39] was used to generate 50 models ranked by Z-DOPE score.[40] These initial models were subsequently filtered down to ten final models based on the volume of the pseudocatalytic cleft internal as measured by POVME 2.0[41]. These models were manually modified to correct for an insertion between the β1 and β2 sheets in the STRADα N-lobe. Models were assessed for continued compatibility with MO25α by identifying clashes between the modeled N-lobe when the C-lobe was aligned with that of the original structure. This analysis suggested that complex formation might favor a relatively small opening of the kinase interlobar hinge, but it was not ultimately used to exclude any models. Finally, the volumes of the entire pseudocatalytic cleft and the allosteric pocket exposed by the GLR flip were calculated using POVME 2.0 using 0.5 Å gridding and custom inclusion volumes. These volumes were compared with both comparably generated models and experimentally determined references of competent kinases for reasonability. Final adjusted models used for screening can be found as supplementary file strada_glr-out_n2m.pdb with details on the ten included models in Table S1.

Virtual screening preparation and implementation

Compound libraries were curated from the ZINC15 compound library, pharmaceutical compounds published or included in patents, and previously synthesized lab compounds. The ZINC15 library (approximately 172 million compounds at the time) was filtered on the bases of molecular weight, logP, and commercial availability (Figure S2A). The roughly seven million starting compounds were filtered using a modified pan assay interference

compounds (PAINS) filter.[42] Compound preparation for screening including tautomer determination was completed using Schrödinger's Epik and LigPrep software from the 2016-3 release.

Prepared compounds screened against the top ten models using Glide with a Van der Waals softening factor of 0.85. Original analysis was performed using Schrödinger's 2016-3 release with results for selected compounds verified using 2019-2. No substantive differences were observed between the results of 2016-3 Glide and 2019-2 Glide. Consensus compound scores across models were calculated using the average of the top three of the ten calculated GlideScores (Figure S2B). Following identification of models that successfully enriched for preliminary hits, consensus scores were recalculated using the average of the three top scores out of the ten selected models. The representative top-scoring poses used in the generation of Figures 3D and S8 can be found in the supplemental file strada_screening_examples.sdf.

Protein expression and purification

STRADα and MO25α in pJ431 and pJ434 vectors (Figure S3) respectively were co-transformed into BL21 DE3 chemically competent cells and selected with both ampicillin and kanamycin. An individual colony was used to grow a starter culture in LB which was in turn used to inoculate the main growth in TB. The main growth was kept at 37 °C in a shaker at 205 RPM until the OD reached 0.6. At that point, the temperature was reduced to 18 °C and 0.5 mM IPTG was added to induce protein expression. The growths were harvested 18–20 hours later through centrifugation at 10,000 RPM for 30 minutes. The pellets were aliquoted into 10 g fractions and stored at −80 °C until use.

Frozen bacterial pellets were thawed in chilled lysis buffer (25 mM Tris pH 7.8; 250 mM NaCl; 5 mM imidazole; 10% glycerol) that had been supplemented with protease inhibitors and lysozyme. The thawed suspension was sonicated for 3 minutes on ice (0.3 seconds on, 2 seconds off) and then centrifuged at 19,000 RPM for one hour at 4 C°. The supernatant was decanted into 4 mL pre-equilibrated cobalt beads and batch bound on a nutator for one hour. The bead-bound sample was loaded onto a column and allowed to flow by gravity. After washing with 4 column volumes of lysis buffer, the protein was eluted from the beads using three successive 6 mL washes in pre-chilled elution buffer (25 mM Tris pH 7.2; 50 mM NaCl; 200 mM imidazole; 10% glycerol). The pooled elution fractions were spiked with EDTA and DTT, diluted to 150 mL, loaded onto a Superloop, and injected onto a 5 mL HiTrap Q column that had been pre-equilibrated with a low salt buffer (25 mM Tris pH 7.8; 0.5 mM EDTA; 2 mM DTT). After a 5-column volume wash at 50 mM NaCl, the protein was eluted through a 20-column volume gradient to 500 mM NaCl. The peak fractions were run using SDS-PAGE to identify those with co-eluted 1:1 STRADα-MO25α complex. Selected fractions were concentrated to 2 mL and run through gel filtration using a pre-equilibrated Superdex 200 16/600 GL column (25 mM Tris pH 7.8; 50 mM NaCl; 2 mM DTT; 1 mM TCEP).

Fluorescence Thermal Stabilization Assay

STRADα/MO25α complex was buffer exchanged into thermal shift buffer (25 mM HEPES pH 7.5; 50 mM NaCl; 2 mM DTT; 1 mM TCEP) and diluted to 5 μM. Compounds were added at 50x concentration to yield 2% final DMSO. After extensive mixing and a 10-minute incubation period, SYPRO Orange dye was added to 10x final concentration. Thorough mixing was once again achieved through repeated pipetting. Samples were transferred to a 384 well plate and equilibrated at 25 °C. A QuantStudio 5 Real-time PCR System was used to run the thermal denaturation protocol. The plate was heated at a rate of 1 °C/minute from 25 °C to 90 °C. The resulting data was analyzed using the ThermoFisher Protein Thermal Shift Program 1.3. Traces were both automatically and manually filtered to remove traces with inadequate baseline statistics relative to controls. The peaks in the first derivative plot were used to quantify thermal shifts.

Protein methylation

Protein samples were prepared for methylation through dialysis into methylation buffer (25 mM Hepes pH 7.5; 50 mM NaCl; 10% glycerol), diluted to 2 mg/mL, and aliquoted into 1 mL fractions in 1.5 mL tubes. 60 μL of 1 M ABC and 80 μL 1M formaldehyde were prepared per 1 mL protein sample. 20 μL 1 M ABC and 40 μL 1 M formaldehyde were added to each protein aliquot and left at 4 °C on a rotisserie nutator for 2 hours. This process was repeated once more. Finally, 10 μL of 1 M formaldehyde was added to each aliquot, and the samples were left on the nutator overnight. The following day, the protein samples were spun to remove precipitate and then collated and concentrated using a concentrator down to 2–5 mL as necessary to reach approximately 10 mg/mL. The samples were loaded onto a pre-equilibrated Superdex 200 16/600 GL column (25 mM Tris pH 7.8; 50 mM NaCl; 2 mM DTT; 1 mM TCEP).

Preparation of specified compounds

Protein samples Compounds 1, 2, and 3 were synthesized based on established procedures;[43] LC-MS and NMR characterization data are included in Figure S4. Compounds 4–8 were generated previously[44] as were Compounds 7 and 8.[45] Compounds 9 and 10 were purchased from Selleck. Compound 11 was also synthesized previously (Scopton et al., in preparation).

Compound clustering

Top hits were clustered by maximum substructure into scaffolds using RDKit[46] and manually inspected for reasonability and consistency of the docking poses. One clinical compound, nilotinib, scored well (higher than linifanib) but was placed in an unlikely pose dissimilar to its crystal pose and was consequently excluded from primary analysis. Nilotinib non-binding was validated in the large-scale FTSA screens. Following identification of the two primary scaffolds (A and B), the set of all compounds to have entered clinical trials were obtained from ChEMBL[31] and compared to the two known scaffolds using the atom pairs topological fingerprint from RDKit[46] with a Sorenson-Dice metric. The highest score for each pharmaceutical compound with any compound from each scaffold were identified and used to rank compounds for chemical similarity.

Results and Discussion

A prerequisite for a kinase or pseudokinase to bind a type II compound is a propensity to adopt a “DFG-out” state.[9] Because this conformational space of pseudokinases is unexplored, we sought corroboration of: 1) the potential pharmacological tractability and efficacy of targeting STRADα with a type II compound through analysis of factors thought to influence “DFG-out” pharmacological accessibility; 2) the extent to which STRADα’s pseudocatalytic cleft substitutions interfere with standard type II compound binding; and 3) the potential biological impact of such an interaction.

The STRADα pseudocatalytic cleft conserves critical biochemical properties despite critical substitutions

Whether STRADα can accommodate a type II compound relies both on its proclivity to adopt a state similar to the “DFG-out” conformation and on the presence of any known factors that can sterically occlude the binding site. The exact factors determining this accessibility are not fully understood. Long duration molecular dynamics simulations have been useful in mapping the energetics of this conformational transition,[47–50] but STRADα contains a 56-residue unstructured loop contiguous to the activation loop that prohibits a reliable analysis. Residue-by-residue comparison between STRADα and *bona fide* kinases can nonetheless suggest the extent of resemblance for STRADα’s energetics and accessibility (Figure 1A–B; Figure S5). One residue in particular that has been suggested to play a role in the “DFG-in” to “DFG-out” transition is the residue immediately prior to the DFG motif.[51] STRADα has a serine (S212) at this position, as is frequently the case in *bona fide* kinases. A different residue, called the gatekeeper because of its strong association with steric hindrance of type II compound binding, is located just before the kinase hinge. STRADα’s gatekeeper residue threonine (T147) is small and is once again among those commonly observed in targeted kinases.

If the “GLR-out” conformation is pharmacologically accessible, then compliance of the STRADα putative binding site with the interactions observed in a consensus type II pharmacophore model would suggest that repurposing a type II compound is a reasonable approach. Previously reported pharmacophore models used in the successful development of type II compounds can be partitioned into three regions: an adenine region, an allosteric region corresponding to the volume revealed by the DFG flip, and a linker region between the two (Figure 1A–B, Figure 2B, Figure S7).[52–53]

The kinase hinge binds the adenine region through highly conserved hydrogen bond and aromatic interactions. Alignment of STRADα with *bona fide* kinases observed crystallographically in complex with type II compounds shows conservation of the hinge residues, specifically of the hydrogen bond accepting S148, the backbone hydrogen bond donating M150, and the aromatic F149 (Figure 1B). The linker pharmacophore primarily interacts with the kinase DFG motif and the conserved salt bridge. STRADα’s GLR could be expected to disrupt this region, but the critical hydrogen bond-donating interaction is with the backbone of aspartate/glycine. Since the amino acid backbone is invariant, this glycine substitution influences rotational dynamics but does not disrupt the hydrogen bond interaction. The kinase salt bridge between the VAIK motif and the αC helix forms a

hydrogen bond with the linker region in the standard pharmacophore model. In STRADα an arginine (R100) substitutes for lysine. This substitution from lysine to arginine is potentially significant, but since the hydrogen bond is specifically with the conserved glutamate from the αC helix, it does not preclude ligand interaction *a priori*. Finally, in conventional kinases the allosteric region interacts with the pocket opened through the flip of the DFG motif phenylalanine. STRADα substitutes leucine for phenylalanine—a substitution observed in almost 10% of *bona fide* kinases.[1] The sidechains of phenylalanine and leucine are both hydrophobic and relatively large (~190 $Å^3$ and ~166 $Å^3$, respectively)[55] suggesting that the revealed allosteric pockets are also probably similar. Thus, the primary kinase interactions of all three pharmacophore regions are largely preserved within STRADα despite the presence of significant active site variation from the kinome consensus.

The STRADα/MO25α/LKB1 complex shows selective evolutionary conservation

Effective pharmacological targeting of any pseudokinase must establish a reasonable rationale for a biological effect. We attempted to determine whether disruption of the activation loop in STRADα might disrupt STRADα/MO25α/LKB1 complex formation and/or LKB1 activation. Previous studies elucidating the structure and function of the STRADα/MO25α/LKB1 complex reported that LKB1 activation by STRADα is disrupted by site-directed mutagenesis of the STRADα activation loop at the interface with LKB1.[23] Most of this interface comprises part of the activation loop. Furthermore, these studies have shown that the interaction of ATP with STRADα is important for assembly of the STRADα/MO25α/LKB1 signaling complex through stabilization of the hinge and positioning of the activation loop.[56]

We sought to corroborate the low tolerance for perturbations in the connected regions responsible for ATP-binding and LKB1 interaction through conservation analysis. The capability of ATP-binding site compounds to modulate the LKB1 interface would predict high evolutionary conservation of the pseudocatalytic cleft and activation loop segment of the LKB1 interface. By the contrapositive, showing poor conservation of either of these regions would potentially refute this proposed pharmacological mechanism. Our analysis of STRADα orthologs across deuterostomes and especially across mammals shows near perfect conservation of the regions of interest in contrast to other solvent-exposed surfaces as shown by ConSURF[57] (Figure 1C–D; Figure S6). This analysis cumulatively suggests that if STRADα can adopt a “GLR-out” state and bind stabilizing type II inhibitors, alterations to downstream signaling should be a predictable outcome.

Chimeric homology modeling produces “GLR-out” models of STRADα

To predict putative type II inhibitors of STRADα using structure-based virtual screening, we first created an ensemble model of STRADα in the “GLR-out” state, which is equivalent to the “DFG-out” state seen in *bona fide* kinases. Here we used an integrated modeling approach to generate initial “GLR-out” models. We first used *DFGmodel*, an ensemble modeling method to model kinases in the “DFG-out” conformation that has been successfully applied to develop type II inhibitors for a range of kinase targets.[38, 45, 58–59] Our initial model combined structural information from the STRADα “GLR-in” crystal structure and the “DFG-out” crystal structures of manually curated serine/threonine kinases

(Figure 2A). The STRADα peptide backbone was assumed to be largely unmoved for regions that are invariant between *bona fide* kinase crystal structures in the "DFG-in" and "DFG-out" conformations. Rotation of the N-lobe around the catalytic cleft, movement of the αC helix, and inversion of the GLR sequence were modeled from eighteen curated serine/threonine "DFG-out" crystal structures. We refined initial models by remodeling the β1 and β2 sheets to incorporate an insertion at the glycine-rich loop relative to all selected reference structures (Figure 1A).

Virtual screening against ensemble "GLR-out" STRADα models enriches for two type II chemical scaffolds

Compounds for virtual screening were curated from four primary sources: 1) the ZINC15 library[60] filtered for lead-like and drug-like properties, commercial availability, and exclusion by PAINS[42] filters; 2) a curated KI library from Selleck; 3) a compound set derived from the SureChEMBL database[61]; and 4) compounds previously developed internally in our lab.[45] Final post-filtering compound totals reached 5,054,661 purchasable unannotated compounds and 2,140 clinical or tool compounds sourced from internal libraries or external pharmaceutical sets. Since there were no validated non-nucleotide small molecule binders to STRADα for any conformation at project initiation, the ensemble could not be trained or filtered using known positives and negatives. All selected compounds were docked against the entire ten-model ensemble of STRADα using Schrödinger's Glide. Ensemble consensus scores were calculated as the mean of the top three out of each compound's ten model scores. This approach considers the high probability that some models are likely to represent physiologically disfavored conformations, and it also minimizes the effect of outlier scores while still requiring top hits to dock well in multiple models. The docking score distributions for the input ZINC15, clinical, and internal lab libraries were calculated and compared, revealing the statistical overperformance of a subset of the internal lab library (Figure 3A). After filtering results to exclude unreasonable poses, analysis of the top hits across all compound sets showed relatively unfavorable scores for the clinical library, although one type II compound, Compound 1 (i.e., the clinical compound ABT-869, also known as linifanib)[62] scored better than the rest. Structural analysis of internal lab compounds revealed significant enrichment of one type II compound series based on a pyrazolopyrimidine scaffold (termed Scaffold B). A selection of compounds for further biophysical validation were chosen out of the top clinical compounds, synthesized derivatives of Compound 1 (termed Scaffold A), derivatives of Scaffold B, and a set of poorly-scoring, chemically diverse compounds with comparable physiochemical properties (Figure 3C–D).

High-ranking compounds thermally stabilize STRADα

Next, we developed assays for compound validation using *in vitro* purified STRADα/MO25α dimer. We designed bacterial expression constructs for STRADα and MO25α based on previously reported crystallography constructs and purified the co-expressed dimeric complex (Figure S9).[56] We optimized a Fluorescence Thermal Stabilization Assay (FTSA) previously applied to study the interactions of STRADα with nucleotides.[22, 63] Following protein and assay validation, we used the FTSA to investigate the interactions of STRADα and STRADα/MO25α complex with the compound set previously identified

through computational docking. STRADα/MO25α complex was used for all large screens and most high replication studies over isolated STRADα because STRADα is constitutively bound to MO25α and preliminary studies failed to reveal meaningful distinctions between isolated and complexed STRADα. Comparison between the measured thermal stabilization of compounds and the docking scores showed excellent agreement across tested compounds (Figure 3B). In this screen, only compounds belonging to Scaffold A or Scaffold B demonstrated significant thermal stabilization of STRADα /MO25α.

ATP-binding inhibition corroborates FTSA results

From this initial FTSA screen we selected a set of ten compounds for more extensive validation. This set consisted of four non-binding clinical compounds (Compounds 7–10), three Scaffold A derivatives including the base clinical compound linifanib (Compounds 1–3), and three Scaffold B derivatives (Compounds 4–6) (Figure 3C; Figure S10). The Scaffold A and Scaffold B compounds share a biphenyl urea motif with the analogs differing in terminal phenyl group substitutions. This biphenyl motif had previously been shown to bind to some *bona fide* kinases in the type II mode;[64] in the case of STRADα, its predicted docking pose is within the type II subpocket that is created by the “GLR-out” flip. The representative compounds for both scaffolds were chosen from among those that exhibited the strongest average stabilization in the initial FTSA screen (Figure 3B). The Scaffold A series was designed and synthesized based on the Scaffold B series, allowing for the selection of derivatives with identical terminal phenyl substitution patterns to maximize internal controls. These representative compounds from Scaffold A and Scaffold B were compared against the set of all compounds that have begun FDA-approved phase 1 clinical trials using an atom pairs topological fingerprint with a Sorenson-Dice similarity metric (Figure S11, Table S3).[65] The two best scoring consensus compounds, Compound 9 (sorafenib) and Compound 10 (regorafenib), were among those with no thermal effect and were consequently included as negative controls due to this high chemical similarity. We noted that Compound 1 (Scaffold A), Compound 5 (Scaffold B), sorafenib, and regorafenib are all high-potency VEGFR2 inhibitors, and we subsequently included two chemically dissimilar VEGFR2 inhibitors, Compound 7 (cabozantinib) and Compound 8 (lenvatinib), in the screening set. Extensive FTSA replication with this set corroborated initial screen findings (Figure 4A). However, the difficulty in correlating thermal stabilization with more pharmacologically relevant parameters such as IC_{50} restricted our analysis to robust Boolean classification of compounds as binders or non-binders.

The FTSA assay permitted high-throughput validation of interactions between compounds and STRADα/MO25α but did not allow interpretation of the binding site location or effective ranking of compound binding. We optimized the ATP-biotin competition assay[66] for STRADα: 1) to assess whether compounds were binding in the pseudocatalytic cleft, 2) to distinguish more clearly strong from weak binders, and 3) to validate FTSA results through an orthogonal approach. In this assay, ATP-biotin conjugates bind to a kinase and covalently transfer the biotin moiety to a nearby lysine residue. Biotin labeling relative to controls was subsequently assessed with a Western blot. This competition assay is conducive to studying pseudokinases because it relies on the presence of lysines in sufficiently close

proximity to interact with the γ-phosphate of ATP rather than on intrinsic catalytic activity.[22]

Application of this assay to STRADα proved unexpectedly difficult because of STRADα's substitution of two proximal ATP-binding site residues from lysine (i.e., K100R and K218L). These lost VAIK and proximal activation loop lysines are among those most frequently observed to conjugate with biotin in a kinome-wide implementation of this assay that used mass spectrometry to measure conjugation.[32] The α-carbons of four lysines (K77, K156, K197, and K239) are located within 9 Å of ATP, but only two (K197 and K239) have sidechains that are positioned reasonably relative to the γ-phosphate (Figure 5B). This potentially attenuates the signal-to-noise ratio for the Western blot assay readout. Comparing Western blot results for STRADα relative to those for previously validated kinases revealed reduced labeling efficiency. This decreases signal over background noise and, by requiring a corresponding increase in protein concentration, decreases maximum assay sensitivity. This assay was still sufficient to robustly distinguish and rank compounds, and the ability of the ATP-biotin probe to label STRADα over background supports interaction between ATP and, most likely, the catalytic loop K197.

The ten-compound set selected from the initial FTSA screen displayed consistent but more stringent results in the ATP-biotin competition assay (Figure 4C). The clinical compounds identified as non-binders by the FTSA screen were consistently statistically indistinguishable from DMSO at inhibiting labeling. Derivatives of Scaffold A showed high variance in inhibition dependent on the concentration of the ATP-biotin probe and the duration of the co-incubation. These compounds at 10 μM were unable to significantly inhibit labeling by 5 μM ATP-biotin probe. However, the derivatives of Scaffold B derivatives significantly inhibited labeling under identical conditions. This suggests that the Scaffold A compounds have an affinity for STRADα comparable but non-superior to the previously reported affinity of ATP while Scaffold B compounds have a much stronger affinity. Previous work using displacement of TNP-ATP to measure binding observed ATP to have K_d of 2.4 μM against STRADα and 24 nM against STRADα/MO25α.[56]

Kinome profiling suggests greater selectivity for Scaffold A over Scaffold B

To determine the relative selectivity of Scaffold A versus Scaffold B compounds, we tested representative compounds containing identical terminal phenyl group substitutions with kinome profiling from Invitrogen and DiscoveRx that respectively evaluate inhibition and binding (Figure 4B; Table S4). Compound 2 (Scaffold A), while less potent than Compound 5 (Scaffold B), showed decreased promiscuity. Both compounds are reported to interact with their primary bona fide kinase targets with IC50 values 2–3 orders of magnitude stronger than that seen with STRADα/MO25α, but Compound 2 (Scaffold A) interacts with fewer kinases more potently than with STRADα/MO25α. The greater potency of Compound 5 (Scaffold B) recommends that scaffold as the preferential tool compound when using purified STRADα/MO25α in vitro.

Surface methylation localizes a Scaffold B compound within the pseudocatalytic cleft

Growing crystals of STRADα/MO25α complex in the presence of identified compounds from both scaffolds proved intractable. Extensive optimization of crystallization conditions for both unmodified and methylated STRADα/MO25α yielded well-diffracting crystals, but a combination of persistent strong merohedral twinning, order-disorder, pseudo-symmetry, and translational non-crystallographic symmetry prevented structure determination through molecular replacement. Without a solved crystal structure, the previous assays could only localize identified compounds to the pseudocatalytic cleft through inhibition of ATP-mediated lysine labeling.

Based on our models, we hypothesized that the most likely binding site and pose for the tested compounds was the pseudocatalytic cleft in the type II pose. We considered two primary alternative hypotheses: 1) compounds bind in a completely different site on the complex, or 2) compounds bind in a non-type II pose within the pseudocatalytic cleft. To examine the first alternative, we looked for alternative binding pockets on the surface of STRADα/MO25α complex using DoGSiteScorer[67] and PyVOL.[68] Using the convenient crystallographic approximation that non-hydrogen atoms can be expected to take up 18–20 $Å^3$, we identified all pockets present with a highly conservative minimum volume of 500 $Å^3$ (Figure 5A). These results suggested that the only non-interface binding site is the pseudocatalytic cleft.

The second alternative allows binding in a type I or type I½ pose. While compounds such as imatinib and sunitinib have been shown to bind in both the type I and type II poses,[69–70] no compound has been shown to bind to both the type I½ and type II poses. Differences between the two compound sets are sufficiently distinct to permit conversion of compounds from one class to the other through SBDD.[71] The prior crystallization of Compound 4 in a type II pose with the *bona fide* kinase c-Src[13] strongly suggests that the consistent linker and allosteric regions of Scaffold A and Scaffold B strongly favor type II poses and disfavor type I½ poses.

We distinguished binding in the type I versus type II pose within the pseudocatalytic cleft by leveraging the substitution of the canonically conserved ATP-binding pocket VAIK motif lysine residue through chemical modification of surface lysines. Previous ATP-biotin results support that at least one nearby surface lysine is close enough to interact with the γ-phosphate of ATP (Figure 5B). Most type II compounds (including Compound 4 in its crystal structure) are positioned more deeply within the catalytic cleft than ATP and type I compounds (Figure 5B). We consequently hypothesized that surface lysine methylation would preferentially impair ATP and type I binding over type II compounds.

We applied this prediction to localize Compound 11, a close derivative of Compounds 2 and 5 differentiated only in the hinge-binding group (Figure 4D), within the pseudocatalytic cleft. We methylated samples of STRADα/MO25α complex in the presence of high concentrations of either ATP or Compound 11. We hypothesized that associated compounds would protect interacting surface lysines within the cleft from methylation. Under this hypothesis, ATP present during the methylation reaction should interfere with the methylation of some subset of the five closest lysine residues, and conversely, the

methylation of these residues should interfere with the binding of ATP to STRADα/MO25α (Figure 5B). If Compound 11 adopts a type II pose, it should interfere with the methylation of any surface lysines to a lesser extent than ATP: it is farther from every lysine and has no polar groups oriented towards these residues. In summary, STRADα/MO25α methylated in the presence of ATP should exhibit an approximately uniform alteration in affinity for both ATP and Compound 11 while STRADα/MO25α methylated in the presence of Compound 11 should have a reduced affinity for ATP relative to Compound 11.

We tested this hypothesis using the FTSA assay (Figure 5C). Under the strong methylating conditions used for this experiment, STRADα/MO25α showed apo baseline destabilization of approximately 10 °C. Compound 11 showed robust stabilization of STRADα/MO25α that was unmethylated, methylated in the presence of ATP, and methylated in the presence of Compound 11. In contrast, ATP stabilized STRADα/MO25α that was unmethylated or methylated in the presence of ATP but failed to significantly stabilize STRADα/MO25α methylated in the presence of Compound 11. This selective failure of ATP to stabilize STRADα/MO25α methylated in the presence of Compound 11 is consistent with a type II binding pose for Scaffold B derivatives.

Conclusions

Our work describes the development of multiple scaffolds with affinity for STRADα. These are the first non-nucleotide small molecules shown to interact with STRADα outside of large-scale pan-kinase proteomic screens. We developed a “GLR-out” ensemble model of STRADα and used it to enrich a large-scale computational screen for putative type II binders. A predicted subset of compounds derived from the two enriched type II scaffolds demonstrated affinity for STRADα through thermal stabilization. Derivatives of Scaffold B showed efficient inhibition of ATP binding. Analyses of surface lysine interactions using the ATP-biotin probe and chemical methylation in the presence of protective compounds supports binding of the representative of Scaffold B, Compound 11, in a type II pose targeting the “GLR-out” state.

Identification of type II compounds that bind to STRADα despite its heavily substituted pseudocatalytic cleft suggests broad potential for such conformation-specific KIs in targeting pseudokinases and lesser-studied kinases. This potential implies the presence of uncharacterized off-target interactions between type II compounds and pseudokinases that could help explain the complex polypharmacological impacts of KIs on signaling networks. These findings suggest that some KIs could be repurposed narrowly for the study of pseudokinase function or more broadly as pseudokinase-targeting adjuvants to current KIs. Our kinome-wide profiling of scaffolds A and B found several common and high-affinity off-targets, including VEGFR2, RET and MAPK13. Notably, testing additional known VEGFR2 inhibitors (eg. sorafenib, regorafenib, cabozantinib, and lenvatinib) against STRADα did not find positive interactions (Figure 4); however, on the basis of the profiling results, perhaps RET and/or MAP3K19 are more appropriate proxies for the identification of distinct STRADα binders.

The impact of type II compounds targeting STRADα on signaling through the LKB1-AMPK-mTOR axis is beyond the scope of this project. However, this structural and conservation analysis of the pseudocatalytic cleft and LKB1 interfaces of STRADα suggest potential for type II compounds to modulate downstream signaling. LKB1 relies on evolutionarily conserved stabilization by the STRADα activation loop for both export from the nucleus and catalytic activation. Perturbations from type II compounds that displace the STRADα activation loop have the resulting potential to disrupt LKB1 activity and/or cellular localization resulting in a decrease in AMPK activity. Decreased AMPK signaling reduces inhibition of cellular anabolism, effectively decoupling cell growth and proliferation from energy availability. Cancer metabolomics further suggests that such metabolic manipulation of cells could have a greater impact within tumor microenvironments due to local ATP depletion through the Warburg effect.

Supplementary Material

Refer to Web version on PubMed Central for supplementary material.

ACKNOWLEDGMENT

We thank Elton Zeqiraj for his advice on the expression and purification and Stuart Aaronson for his suggestions for compound localization. We acknowledge Ross Cagan and Andres Maldonado for their advice throughout the project.

Funding Sources

Dar laboratory members are supported by innovation awards from the NIH (1DP2CA186570-01) and the Damon Runyan Rachleff Foundation, as well as NIH grants 1R01CA227636 and 5U54OD020353 and NCI grant P30 CA196521 to the Tisch Cancer Institute. R.H.B.S. is also supported by NIH grant T32HD075735. A.C.D. is a Pew-Stewart Scholar in Cancer Research and Young Investigator of the Pershing-Square Sohn Cancer Research Alliance. Research reported in this paper was supported by the Office of Research Infrastructure of the National Institutes of Health under award numbers S10OD018522 and S10OD026880.

ABBREVIATIONS

ABC	dimethylamine-borane complex
AMPK	5’ adenosine monophosphate-activated protein kinase
ATP	adenosine triphosphate
c-Src	cellular sarcoma
DFG	aspartate-phenylalanine-glycine
DMSO	dimethyl sulfoxide
DOPE	discrete optimized protein energy
DTT	dithiothreitol
EDTA	ethylenediaminetetraacetic acid
ERK	extracellular signal-regulated kinase

FDA	U.S. Food and Drug Administration
FTSA	fluorescence thermal stabilization assay
GK	gatekeeper
GLR	glycine-leucine-arginine
HEPES	4-(−2-hydroxyethyl)-1-piperazineethanesulfonic acid
IPTG	isopropyl β-d-1-thiogalactopyranoside
KI	kinase inhibitor
KSR2	kinase suppressor of Ras 2
LB	lysogeny broth
LC-MS	liquid chromatography mass spectrometry
LKB1	serine-threonine kinase B1
MAPK	mitogen-activated protein kinase
MARK	MAP/microtubule affinity-regulating kinase
MO25α	calcium-binding protein 39
mTOR	mammalian target of rapamycin
N-lobe	N-terminal lobe
NMR	nuclear magnetic resonance
OD	optical density
PAINS	pan assay interference compounds
STE20	serine-threonine kinase 20
STRADα	STE20-related adaptor protein alpha
TB	terrific broth
TCEP	tris(2-carboxyehtyl)phosphine
VEGFR2	vascular endothelial growth factor receptor 2

REFERENCES

1. Manning G; Whyte DB; Martinez R; Hunter T; Sudarsanam S, The protein kinase complement of the human genome. Science 2002, 298 (5600), 1912–34. [PubMed: 12471243]
2. Manning G; Plowman GD; Hunter T; Sudarsanam S, Evolution of protein kinase signaling from yeast to man. Trends Biochem Sci 2002, 27 (10), 514–20. [PubMed: 12368087]

3. Kwon A; Scott S; Taujale R; Yeung W; Kochut KJ; Eyers PA; Kannan N, Tracing the origin and evolution of pseudokinases across the tree of life. Sci Signal 2019, 12 (578), eaav3810. [PubMed: 31015289]

4. Boudeau J; Miranda-Saavedra D; Barton GJ; Alessi DR, Emerging roles of pseudokinases. Trends Cell Biol 2006, 16 (9), 443–52. [PubMed: 16879967]

5. Eyers PA; Murphy JM, Dawn of the dead: protein pseudokinases signal new adventures in cell biology. Biochem Soc Trans 2013, 41 (4), 969–74. [PubMed: 23863165]

6. Endicott JA; Noble ME; Johnson LN, The structural basis for control of eukaryotic protein kinases. Annu Rev Biochem 2012, 81 (1), 587–613. [PubMed: 22482904]

7. Bailey FP; Byrne DP; Oruganty K; Eyers CE; Novotny CJ; Shokat KM; Kannan N; Eyers PA, The Tribbles 2 (TRB2) pseudokinase binds to ATP and autophosphorylates in a metal-independent manner. Biochem J 2015, 467 (1), 47–62. [PubMed: 25583260]

8. Huse M; Kuriyan J, The conformational plasticity of protein kinases. Cell 2002, 109 (3), 275–82. [PubMed: 12015977]

9. Seeliger MA; Ranjitkar P; Kasap C; Shan Y; Shaw DE; Shah NP; Kuriyan J; Maly DJ, Equally potent inhibition of c-Src and Abl by compounds that recognize inactive kinase conformations. Cancer Res 2009, 69 (6), 2384–92. [PubMed: 19276351]

10. Mobitz H, The ABC of protein kinase conformations. Biochim Biophys Acta 2015, 1854 (10 Pt B), 1555–66. [PubMed: 25839999]

11. Shan Y; Seeliger MA; Eastwood MP; Frank F; Xu H; Jensen MO; Dror RO; Kuriyan J; Shaw DE, A conserved protonation-dependent switch controls drug binding in the Abl kinase. Proc Natl Acad Sci U S A 2009, 106 (1), 139–44. [PubMed: 19109437]

12. Roskoski R Jr., Classification of small molecule protein kinase inhibitors based upon the structures of their drug-enzyme complexes. Pharmacological research 2016, 103, 26–48. [PubMed: 26529477]

13. Dar AC; Lopez MS; Shokat KM, Small molecule recognition of c-Src via the Imatinib-binding conformation. Chemistry & biology 2008, 15 (10), 1015–22. [PubMed: 18940662]

14. Zhao Z; Wu H; Wang L; Liu Y; Knapp S; Liu Q; Gray NS, Exploration of type II binding mode: A privileged approach for kinase inhibitor focused drug discovery? ACS Chem Biol 2014, 9 (6), 1230–41. [PubMed: 24730530]

15. Kufareva I; Abagyan R, Type-II kinase inhibitor docking, screening, and profiling using modified structures of active kinase states. J Med Chem 2008, 51 (24), 7921–32. [PubMed: 19053777]

16. Rahman R; Ung PM; Schlessinger A, KinaMetrix: a web resource to investigate kinase conformations and inhibitor space. Nucleic Acids Res 2019, 47 (D1), D361–D366. [PubMed: 30321373]

17. Sheetz JB; Mathea S; Karvonen H; Malhotra K; Chatterjee D; Niininen W; Perttila R; Preuss F; Suresh K; Stayrook SE; Tsutsui Y; Radhakrishnan R; Ungureanu D; Knapp S; Lemmon MA, Structural Insights into Pseudokinase Domains of Receptor Tyrosine Kinases. Mol Cell 2020, 79 (3), 390–405 e7. [PubMed: 32619402]

18. Dhawan NS; Scopton AP; Dar AC, Small molecule stabilization of the KSR inactive state antagonizes oncogenic Ras signalling. Nature 2016, 537 (7618), 112–116. [PubMed: 27556948]

19. Ung PM; Rahman R; Schlessinger A, Redefining the Protein Kinase Conformational Space with Machine Learning. Cell Chem Biol 2018, 25 (7), 916–924 e2. [PubMed: 29861272]

20. Khan ZM; Real AM; Marsiglia WM; Chow A; Duffy ME; Yerabolu JR; Scopton AP; Dar AC, Structural basis for the action of the drug trametinib at KSR-bound MEK. Nature 2020.

21. Boudeau J; Baas AF; Deak M; Morrice NA; Kieloch A; Schutkowski M; Prescott AR; Clevers HC; Alessi DR, MO25alpha/beta interact with STRADalpha/beta enhancing their ability to bind, activate and localize LKB1 in the cytoplasm. EMBO J 2003, 22 (19), 5102–14. [PubMed: 14517248]

22. Murphy JM; Zhang Q; Young SN; Reese ML; Bailey FP; Eyers PA; Ungureanu D; Hammaren H; Silvennoinen O; Varghese LN; Chen K; Tripaydonis A; Jura N; Fukuda K; Qin J; Nimchuk Z; Mudgett MB; Elowe S; Gee CL; Liu L; Daly RJ; Manning G; Babon JJ; Lucet IS, A robust methodology to subclassify pseudokinases based on their nucleotide-binding properties. Biochem J 2014, 457 (2), 323–34. [PubMed: 24107129]

23. Zeqiraj E; Filippi BM; Deak M; Alessi DR; van Aalten DM, Structure of the LKB1-STRAD-MO25 complex reveals an allosteric mechanism of kinase activation. Science 2009, 326 (5960), 1707–11. [PubMed: 19892943]
24. Shackelford DB; Shaw RJ, The LKB1-AMPK pathway: metabolism and growth control in tumour suppression. Nat Rev Cancer 2009, 9 (8), 563–75. [PubMed: 19629071]
25. Kullmann L; Krahn MP, Controlling the master-upstream regulation of the tumor suppressor LKB1. Oncogene 2018, 37 (23), 3045–3057. [PubMed: 29540834]
26. Woods A; Johnstone SR; Dickerson K; Leiper FC; Fryer LG; Neumann D; Schlattner U; Wallimann T; Carlson M; Carling D, LKB1 is the upstream kinase in the AMP-activated protein kinase cascade. Curr Biol 2003, 13 (22), 2004–8. [PubMed: 14614828]
27. Shaw RJ; Kosmatka M; Bardeesy N; Hurley RL; Witters LA; DePinho RA; Cantley LC, The tumor suppressor LKB1 kinase directly activates AMP-activated kinase and regulates apoptosis in response to energy stress. Proc Natl Acad Sci U S A 2004, 101 (10), 3329–35. [PubMed: 14985505]
28. Hawley SA; Boudeau J; Reid JL; Mustard KJ; Udd L; Makela TP; Alessi DR; Hardie DG, Complexes between the LKB1 tumor suppressor, STRAD alpha/beta and MO25 alpha/beta are upstream kinases in the AMP-activated protein kinase cascade. J Biol 2003, 2 (4), 28. [PubMed: 14511394]
29. Goodwin JM; Svensson RU; Lou HJ; Winslow MM; Turk BE; Shaw RJ, An AMPK-independent signaling pathway downstream of the LKB1 tumor suppressor controls Snail1 and metastatic potential. Mol Cell 2014, 55 (3), 436–50. [PubMed: 25042806]
30. Lizcano JM; Goransson O; Toth R; Deak M; Morrice NA; Boudeau J; Hawley SA; Udd L; Makela TP; Hardie DG; Alessi DR, LKB1 is a master kinase that activates 13 kinases of the AMPK subfamily, including MARK/PAR-1. EMBO J 2004, 23 (4), 833–43. [PubMed: 14976552]
31. Gaulton A; Bellis LJ; Bento AP; Chambers J; Davies M; Hersey A; Light Y; McGlinchey S; Michalovich D; Al-Lazikani B; Overington JP, ChEMBL: a large-scale bioactivity database for drug discovery. Nucleic Acids Res 2012, 40 (Database issue), D1100–7. [PubMed: 21948594]
32. Klaeger S; Heinzlmeir S; Wilhelm M; Polzer H; Vick B; Koenig PA; Reinecke M; Ruprecht B; Petzoldt S; Meng C; Zecha J; Reiter K; Qiao H; Helm D; Koch H; Schoof M; Canevari G; Casale E; Depaolini SR; Feuchtinger A; Wu Z; Schmidt T; Rueckert L; Becker W; Huenges J; Garz AK; Gohlke BO; Zolg DP; Kayser G; Vooder T; Preissner R; Hahne H; Tonisson N; Kramer K; Gotze K; Bassermann F; Schlegl J; Ehrlich HC; Aiche S; Walch A; Greif PA; Schneider S; Felder ER; Ruland J; Medard G; Jeremias I; Spiekermann K; Kuster B, The target landscape of clinical kinase drugs. Science 2017, 358 (6367), eaan4368. [PubMed: 29191878]
33. Armougom F; Moretti S; Poirot O; Audic S; Dumas P; Schaeli B; Keduas V; Notredame C, Expresso: automatic incorporation of structural information in multiple sequence alignments using 3D-Coffee. Nucleic Acids Res 2006, 34 (Web Server issue), W604–W608. [PubMed: 16845081]
34. El-Gebali S; Mistry J; Bateman A; Eddy SR; Luciani A; Potter SC; Qureshi M; Richardson LJ; Salazar GA; Smart A; Sonnhammer ELL; Hirsh L; Paladin L; Piovesan D; Tosatto SCE; Finn RD, The Pfam protein families database in 2019. Nucleic Acids Res 2018, 47 (D1), D427–D432.
35. Li H; Coghlan A; Ruan J; Coin LJ; Hériché JK; Osmotherly L; Li R; Liu T; Zhang Z; Bolund L; Wong GK; Zheng W; Dehal P; Wang J; Durbin R, TreeFam: a curated database of phylogenetic trees of animal gene families. Nucleic Acids Res 2006, 34 (Database issue), D572–80. [PubMed: 16381935]
36. Madeira F; Park YM; Lee J; Buso N; Gur T; Madhusoodanan N; Basutkar P; Tivey ARN; Potter SC; Finn RD; Lopez R, The EMBL-EBI search and sequence analysis tools APIs in 2019. Nucleic Acids Res 2019, 47 (W1), W636–W641. [PubMed: 30976793]
37. Ashkenazy H; Abadi S; Martz E; Chay O; Mayrose I; Pupko T; Ben-Tal N, ConSurf 2016: an improved methodology to estimate and visualize evolutionary conservation in macromolecules. Nucleic Acids Res 2016, 44 (W1), W344–W350. [PubMed: 27166375]
38. Ung PM; Schlessinger A, DFGmodel: predicting protein kinase structures in inactive states for structure-based discovery of type-II inhibitors. ACS Chem Biol 2015, 10 (1), 269–78. [PubMed: 25420233]

39. Sali A; Blundell TL, Comparative protein modelling by satisfaction of spatial restraints. J Mol Biol 1993, 234 (3), 779–815. [PubMed: 8254673]
40. Shen M-Y; Sali A, Statistical potential for assessment and prediction of protein structures. Protein Sci 2006, 15 (11), 2507–2524. [PubMed: 17075131]
41. Durrant JD; Votapka L; Sørensen J; Amaro RE, POVME 2.0: An Enhanced Tool for Determining Pocket Shape and Volume Characteristics. Journal of chemical theory and computation 2014, 10 (11), 5047–5056. [PubMed: 25400521]
42. Baell JB; Holloway GA, New substructure filters for removal of pan assay interference compounds (PAINS) from screening libraries and for their exclusion in bioassays. J Med Chem 2010, 53 (7), 2719–40. [PubMed: 20131845]
43. Dai Y; Hartandi K; Ji Z; Ahmed AA; Albert DH; Bauch JL; Bouska JJ; Bousquet PF; Cunha GA; Glaser KB; Harris CM; Hickman D; Guo J; Li J; Marcotte PA; Marsh KC; Moskey MD; Martin RL; Olson AM; Osterling DJ; Pease LJ; Soni NB; Stewart KD; Stoll VS; Tapang P; Reuter DR; Davidsen SK; Michaelides MR, Discovery of N-(4-(3-Amino-1H-indazol-4-yl)phenyl)-N'-(2-fluoro-5-methylphenyl)urea (ABT-869), a 3-Aminoindazole-Based Orally Active Multitargeted Receptor Tyrosine Kinase Inhibitor. Journal of Medicinal Chemistry 2007, 50 (7), 1584–1597. [PubMed: 17343372]
44. Yu JX; Craig AJ; Duffy ME; Villacorta-Martin C; Miguela V; Ruiz de Galarreta M; Scopton AP; Silber L; Maldonado AY; Rialdi A; Guccione E; Lujambio A; Villanueva A; Dar AC, Phenotype-Based Screens with Conformation-Specific Inhibitors Reveal p38 Gamma and Delta as Targets for HCC Polypharmacology. Mol Cancer Ther 2019, 18 (9), 1506–1519. [PubMed: 31213506]
45. Sonoshita M; Scopton AP; Ung PMU; Murray MA; Silber L; Maldonado AY; Real A; Schlessinger A; Cagan RL; Dar AC, A whole-animal platform to advance a clinical kinase inhibitor into new disease space. Nature chemical biology 2018, 14 (3), 291–298. [PubMed: 29355849]
46. Landrum G, RDKit: Open-source cheminformatics. 2006.
47. Meng Y; Lin YL; Roux B, Computational study of the "DFG-flip" conformational transition in c-Abl and c-Src tyrosine kinases. J Phys Chem B 2015, 119 (4), 1443–56. [PubMed: 25548962]
48. Cyphers S; Ruff EF; Behr JM; Chodera JD; Levinson NM, A water-mediated allosteric network governs activation of Aurora kinase A. Nature chemical biology 2017, 13 (4), 402–408. [PubMed: 28166210]
49. Casasnovas R; Limongelli V; Tiwary P; Carloni P; Parrinello M, Unbinding Kinetics of a p38 MAP Kinase Type II Inhibitor from Metadynamics Simulations. J Am Chem Soc 2017, 139 (13), 4780–4788. [PubMed: 28290199]
50. Tsai CC; Yue Z; Shen J, How Electrostatic Coupling Enables Conformational Plasticity in a Tyrosine Kinase. J Am Chem Soc 2019, 141 (38), 15092–15101. [PubMed: 31476863]
51. Hari SB; Merritt EA; Maly DJ, Sequence determinants of a specific inactive protein kinase conformation. Chemistry & biology 2013, 20 (6), 806–15. [PubMed: 23790491]
52. Liu Y; Gray NS, Rational design of inhibitors that bind to inactive kinase conformations. Nature chemical biology 2006, 2 (7), 358–64. [PubMed: 16783341]
53. Okram B; Nagle A; Adrian FJ; Lee C; Ren P; Wang X; Sim T; Xie Y; Wang X; Xia G; Spraggon G; Warmuth M; Liu Y; Gray NS, A general strategy for creating "inactive-conformation" abl inhibitors. Chemistry & biology 2006, 13 (7), 779–86. [PubMed: 16873026]
54. Madeira F; Park YM; Lee J; Buso N; Gur T; Madhusoodanan N; Basutkar P; Tivey ARN; Potter SC; Finn RD; Lopez R, The EMBL-EBI search and sequence analysis tools APIs in 2019. Nucleic Acids Res 2019, 47 (W1), W636–W641. [PubMed: 30976793]
55. Perkins SJ, Protein volumes and hydration effects. The calculations of partial specific volumes, neutron scattering matchpoints and 280-nm absorption coefficients for proteins and glycoproteins from amino acid sequences. Eur J Biochem 1986, 157 (1), 169–80. [PubMed: 3709531]
56. Zeqiraj E; Filippi BM; Goldie S; Navratilova I; Boudeau J; Deak M; Alessi DR; van Aalten DM, ATP and MO25alpha regulate the conformational state of the STRADalpha pseudokinase and activation of the LKB1 tumour suppressor. PLoS Biol 2009, 7 (6), e1000126. [PubMed: 19513107]

57. Ashkenazy H; Abadi S; Martz E; Chay O; Mayrose I; Pupko T; Ben-Tal N, ConSurf 2016: an improved methodology to estimate and visualize evolutionary conservation in macromolecules. Nucleic Acids Res 2016, 44 (W1), W344–50. [PubMed: 27166375]
58. Dar AC; Das TK; Shokat KM; Cagan RL, Chemical genetic discovery of targets and anti-targets for cancer polypharmacology. Nature 2012, 486 (7401), 80–4. [PubMed: 22678283]
59. Ung PMU; Sonoshita M; Scopton AP; Dar AC; Cagan RL; Schlessinger A, Integrated computational and Drosophila cancer model platform captures previously unappreciated chemicals perturbing a kinase network. PLoS Comput Biol 2019, 15 (4), e1006878. [PubMed: 31026276]
60. Sterling T; Irwin JJ, ZINC 15--Ligand Discovery for Everyone. J Chem Inf Model 2015, 55 (11), 2324–37. [PubMed: 26479676]
61. Christmann-Franck S; van Westen GJ; Papadatos G; Beltran Escudie F; Roberts A; Overington JP; Domine D, Unprecedently Large-Scale Kinase Inhibitor Set Enabling the Accurate Prediction of Compound-Kinase Activities: A Way toward Selective Promiscuity by Design? J Chem Inf Model 2016, 56 (9), 1654–75. [PubMed: 27482722]
62. Albert DH; Tapang P; Magoc TJ; Pease LJ; Reuter DR; Wei RQ; Li J; Guo J; Bousquet PF; Ghoreishi-Haack NS; Wang B; Bukofzer GT; Wang YC; Stavropoulos JA; Hartandi K; Niquette AL; Soni N; Johnson EF; McCall JO; Bouska JJ; Luo Y; Donawho CK; Dai Y; Marcotte PA; Glaser KB; Michaelides MR; Davidsen SK, Preclinical activity of ABT-869, a multitargeted receptor tyrosine kinase inhibitor. Mol Cancer Ther 2006, 5 (4), 995–1006. [PubMed: 16648571]
63. Scott AD, Chapter 8. Fluorescent Thermal Shift Assays for Identifying Small Molecule Ligands. In Biophysical Techniques in Drug Discovery, The Royal Society of Chemistry: 2017; pp 208–238.
64. Tan L; Nomanbhoy T; Gurbani D; Patricelli M; Hunter J; Geng J; Herhaus L; Zhang J; Pauls E; Ham Y; Choi HG; Xie T; Deng X; Buhrlage SJ; Sim T; Cohen P; Sapkota G; Westover KD; Gray NS, Discovery of type II inhibitors of TGFbeta-activated kinase 1 (TAK1) and mitogen-activated protein kinase kinase kinase kinase 2 (MAP4K2). J Med Chem 2015, 58 (1), 183–96. [PubMed: 25075558]
65. Carhart RE; Smith DH; Venkataraghavan R, Atom pairs as molecular features in structure-activity studies: definition and applications. J Chem Inf Model 1985, 25 (2), 64–73.
66. Patricelli MP; Szardenings AK; Liyanage M; Nomanbhoy TK; Wu M; Weissig H; Aban A; Chun D; Tanner S; Kozarich JW, Functional interrogation of the kinome using nucleotide acyl phosphates. Biochemistry 2007, 46 (2), 350–8. [PubMed: 17209545]
67. Volkamer A; Kuhn D; Rippmann F; Rarey M, DoGSiteScorer: a web server for automatic binding site prediction, analysis and druggability assessment. Bioinformatics (Oxford, England) 2012, 28 (15), 2074–5.
68. Smith RHB; Dar AC; Schlessinger A, PyVOL: a PyMOL plugin for visualization, comparison, and volume calculation of drug-binding sites. bioRxiv 2019, 816702.
69. Atwell S; Adams JM; Badger J; Buchanan MD; Feil IK; Froning KJ; Gao X; Hendle J; Keegan K; Leon BC, A novel mode of Gleevec binding is revealed by the structure of spleen tyrosine kinase. Journal of Biological Chemistry 2004, 279 (53), 55827–55832.
70. Gajiwala KS; Wu JC; Christensen J; Deshmukh GD; Diehl W; DiNitto JP; English JM; Greig MJ; He YA; Jacques SL; Lunney EA; McTigue M; Molina D; Quenzer T; Wells PA; Yu X; Zhang Y; Zou A; Emmett MR; Marshall AG; Zhang HM; Demetri GD, KIT kinase mutants show unique mechanisms of drug resistance to imatinib and sunitinib in gastrointestinal stromal tumor patients. Proc Natl Acad Sci U S A 2009, 106 (5), 1542–7. [PubMed: 19164557]
71. Muraoka T; Ide M; Irie M; Morikami K; Miura T; Nishihara M; Kashiwagi H, Development of a method for converting a TAK1 type I inhibitor into a type II or c-helix-out inhibitor by structure-based drug design (SBDD). Chemical and Pharmaceutical Bulletin 2016, 64 (11), 1622–1629. [PubMed: 27803473]

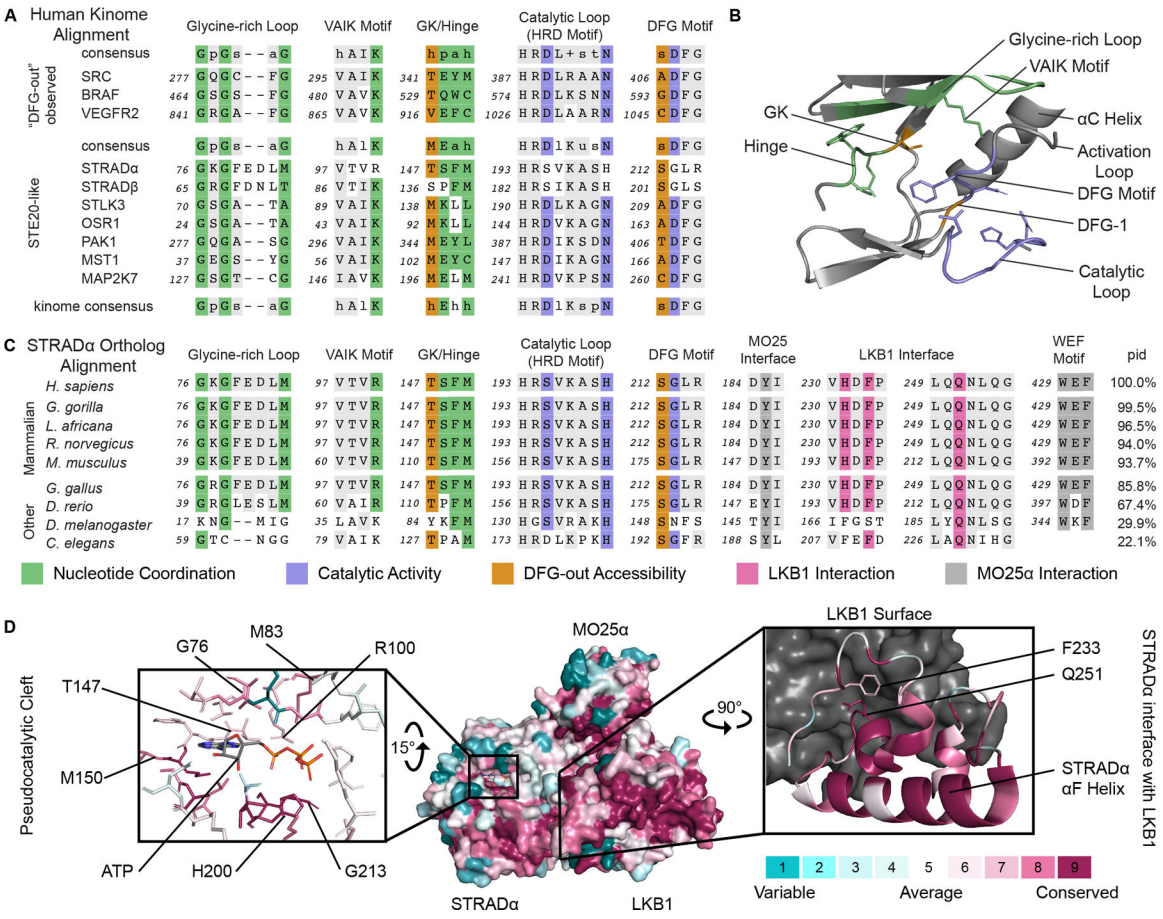

Figure 1.

Structural conservation of STRADα relative to orthologs and the human kinome. **A.** Representative sequences from the full alignment of STRADα with *bona fide* human protein kinases (Figure S5). Also shown are the 60% consensus sequences derived from the kinome and both displayed subgroups using MView[54] consensus patterns. Conserved kinase sequences are shown and shaded by functional assignment and conservation. **B.** An example annotated catalytic cleft showing the position of selected conserved motifs for BRAF in the "DFG-out" conformation (PDB code: 1UWH). **C.** Alignment of STRADα orthologs from selected mammalian and other eukaryotic species displayed along with percent identity calculations (Figure S6). Sequences importance to interaction with LKB1 and MO25α are shown are also shown. **D.** The trimeric STRADα/MO25α/LKB1 complex with evolutionary conservation of chordate orthologs mapped onto the molecular surfaces. Insets show greater detail for STRADα at the pseudocatalytic cleft and the interface with LKB1.

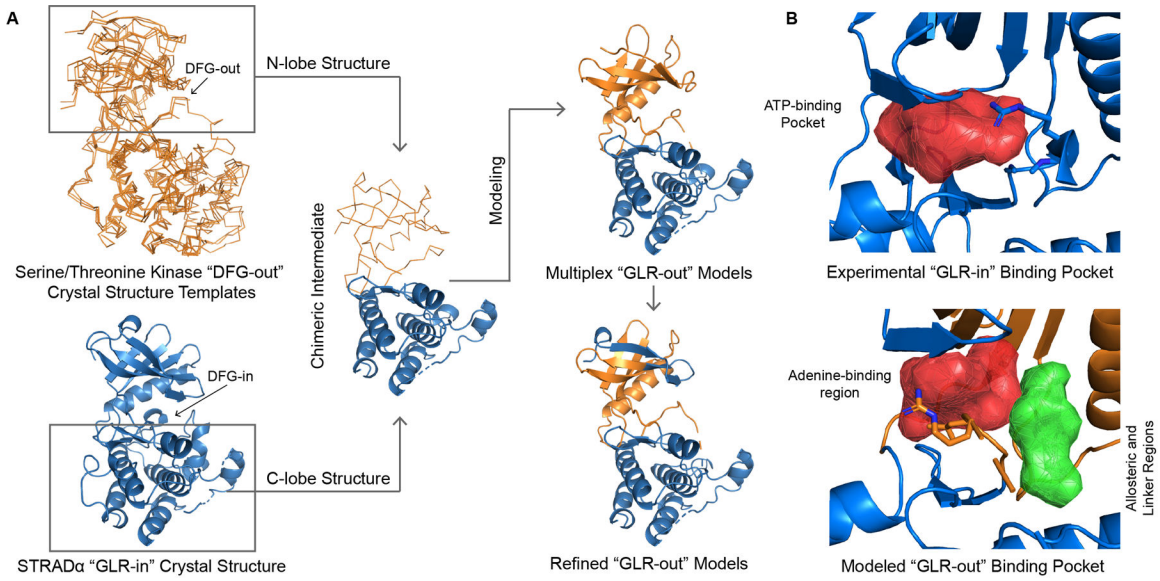

Figure 2.

Generation and visualization of the STRADα "GLR-out" ensemble models. **A.** Modeling procedure to predict "GLR-out" conformations of STRADα through homology modeling of a chimeric intermediate. Characterization of top models is shown in Table S1. **B.** Visualization of the pseudocatalytic cleft binding pockets present in the crystal structure (PDB code: 3GNI) of STRADα in the "GLR-in" conformation and a representative model in the "GLR-out" conformation. The subpockets corresponding to the adenine-binding (red) and combined allosteric and linker (green) pharmacophore regions are shown.

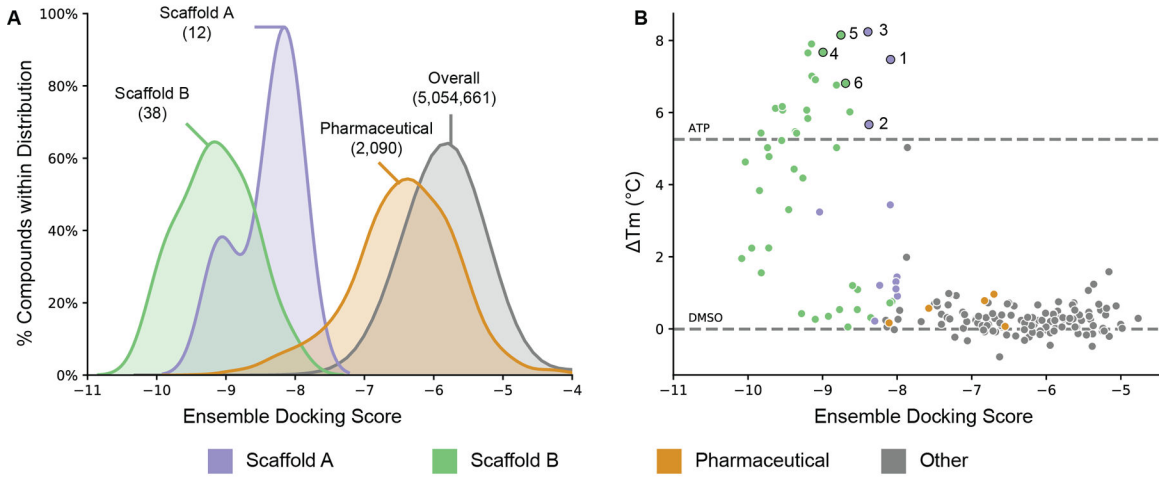

C

Scaffold A

Compound	R_1	R_2	R_3
1	CH_3	H	F
2	CF_3	H	F
3	CF_3	H	H

Scaffold B

Compound	R_1	R_2	R_3
4	CF_3	H	H
5	CF_3	H	F
6	CF_3	Cl	H

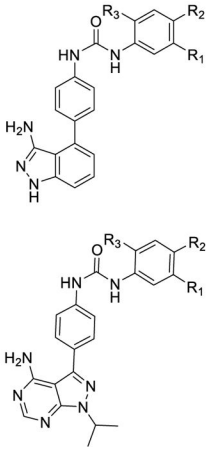

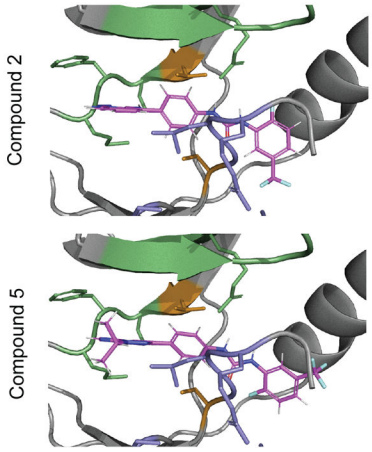

Figure 3.

Virtual and FTSA screening results with the structures and docking poses of selected compounds. **A.** Distribution of consensus ensemble docking scores calculated from 10 models for datasets of Scaffold A, Scaffold B, and pharmaceutically published compounds shown relative to the overall distribution drawn from the ZINC15 database (selected scores in Table S2). **B.** Plot of measured FTSA thermal stabilization of STRADα in the presence of 40 μM compound against calculated consensus ensemble docking scores. **C.** Structure of the Scaffold A and Scaffold B with the specific substitutions of labeled groups shown for highlighted compounds. **D.** Representative docking poses for each scaffold colored according to the scheme from Figure 1A–C. Docking poses for other selected compounds are shown in Figure S8.

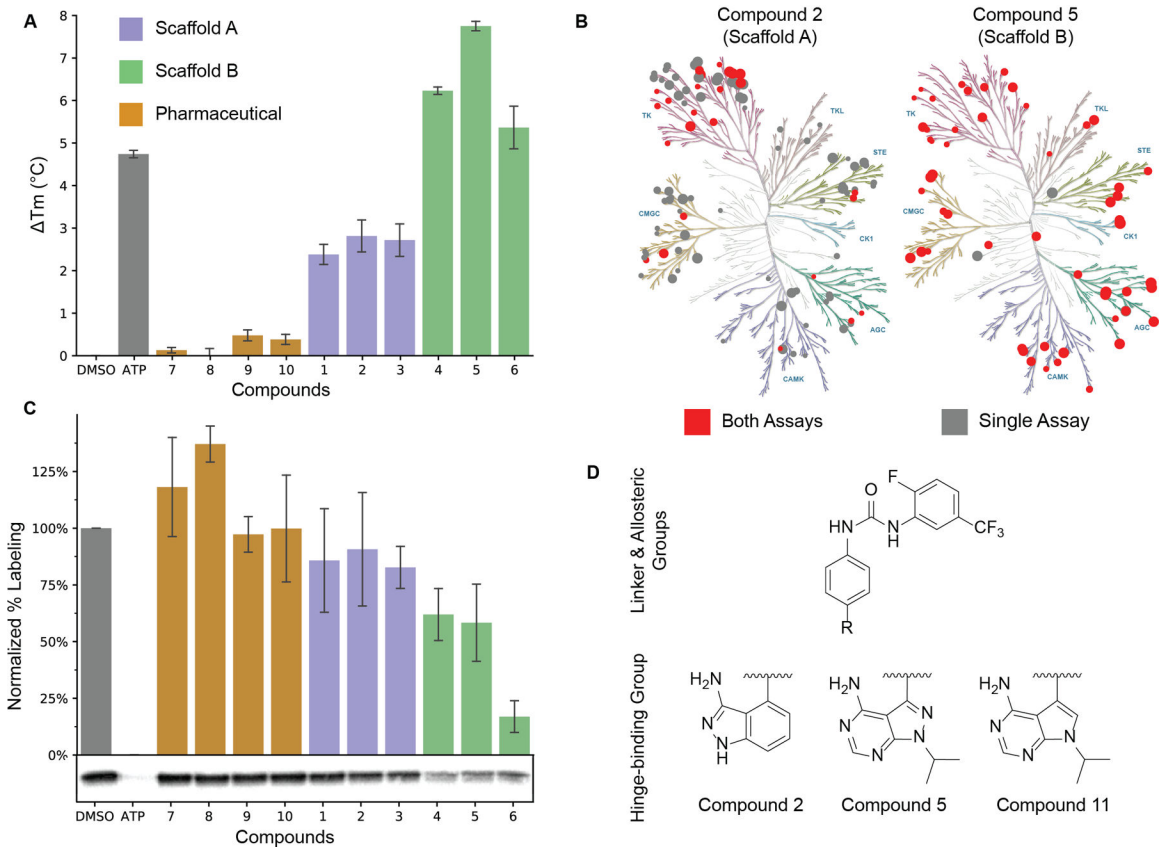

Figure 4.

Biochemical characterization and comparison of selected compounds. **A.** Quantitation of thermal stabilizations caused by a selection of control, pharmaceutical, Scaffold A, and Scaffold B compounds. **B.** Kinome inhibition profiles at 1 μM for Compound 2 and Compound 5 as respective representatives of Scaffolds A and B. Inhibition of >25% is shown with circle size proportional to strength of inhibition (Table S4). **C.** Characteristic blot and quantitation for competitive inhibition measurement of the same compound selection at 10 μM using an ATP-biotin probe (Figure S12) **D.** Structures of Compounds 2, 5 and 11 for comparison (Figure S10).

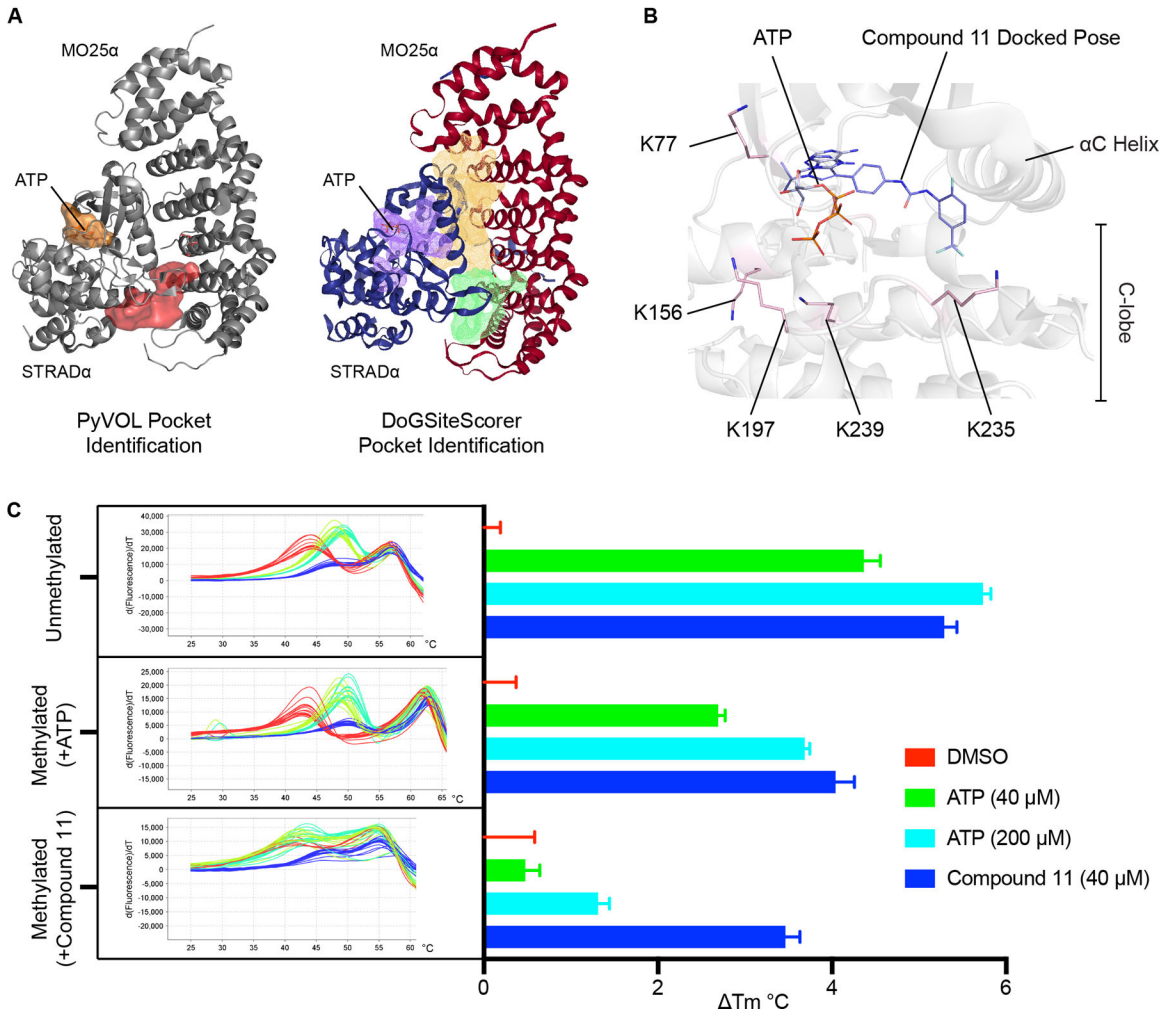

Figure 5:

Surface modification localization of Compound 11 binding to STRADα. **A.** Potential binding pockets identified in the dimeric complex by PyVOL and DoGSiteScorer with volumes of at least 500 Å^3. The pseudocatalytic clefts are marked with bound ATP. **B.** Structure of the pseudocatalytic cleft of STRADα showing the positions of all surface lysine residues within 12 Å of the nearest atom in the crystallographically-observed ATP or superimposed binding pose of Compound 11. Note the tight superposition of the hinge-binding moiety of Compound 11 with the adenine of ATP. **C.** Experimental traces and quantitation showing FTSA thermal stabilization of unmethylated STRADα/MO25α, STRADα/MO25α methylated in the presence of ATP, and STRADα/MO25α methylated in the presence of Compound 11 by DMSO, ATP, and Compound 11. Quantitation is specific for the STRADα melting event.